Structures 69 (2024) 107413

Contents lists available at ScienceDirect

Structures

journal homepage: www.elsevier.com/locate/structures

A novel experimental method for bolt stress distribution during the assembly process☆

Zhixiang Li [a], Zhen Zhao [a,*], Jiaying Zhang [a], Caishan Liu [b]

[a] School of Aeronautic Science and Engineering, Beihang University, Beijing 100191, China
[b] State Key Laboratory for Turbulence and Complex Systems, College of Engineering, Peking University, Beijing 100871, China

ARTICLE INFO

MSC:
74-05

Keywords:
Bolt assembly
Stress distribution
OFDR technique
Axial force gain factor

ABSTRACT

Bolt fasteners play a crucial role in modern engineering equipment, and understanding the stress distribution in the bolt during the assembly process is essential for enhancing its reliability. However, traditional experimental methods based on the principle of photoelasticity may not accurately reflect the actual assembly process and engineering materials. To address this issue, a novel experimental approach is proposed in this paper, which utilizes optical fibers to measure stress in the bolt during the assembly process. By affixing an optical fiber to the inside of the bolt and employing the optical frequency domain reflectometry (OFDR) technique, the axial stress distribution in the bolt can be obtained. In addition, the concept of an axial force gain factor is introduced to establish the relationship between the maximum axial force and preload. It is found that the calculated maximum axial force of the bolt is approximately 1.4 to 1.5 times the preload. The experimental results show that the stress distribution obtained through the proposed method is consistent with conventional photoelasticity experiments. Furthermore, a comparison with previous studies validates the accuracy of the experimental findings. The experimental approach presented in this paper can realize the real-time measurement of bolt stress distribution, which is of great significance for engineering application.

1. Introduction

Bolt fasteners are commonly utilized in modern engineering equipment, such as aviation spacecraft, wind turbine spindles, petrochemical pipeline docking and so on. In practical applications, the strength and stability of bolt fasteners are of utmost importance when subjected to loads, but the behavior of the contact surface is extremely intricate. Understanding the stress and strain distribution in th bolt during the assembly process is crucial for enhancing its reliability and preventing failures [1]. However, accurately modeling the bolt assembly process is extremely challenging due to the complexity of inter-thread contact and friction.

Extensive experimental studies on the stress distribution in bolts have been conducted. One of the main measurement methods is the photoelasticity test [2]. The experimental method harnesses the characteristic of birefringence observed in certain transparent materials. Birefringence is an optical property where light passing through a given material exhibits two different refractive indices. These refractive indices are closely related to the localized stress state inside the material. Den Hartog performed two-dimensional (2D) photoelastic experiments using a celluloid plate model of four threads with a square thread form. His findings indicated that the first two threads took the majority of the load [3]. Hetenyi conducted three-dimensional (3D) photoelastic experiments using four 3D double-headed bolts machined from Bakelite and six different designs of nuts and identified the stress concentration phenomenon [4]. Brown and Hickson conducted similar experiments to Hetenyi using a new photoelastic material called Fosterite [5]. Kenny and Patterson use an automatic recording microdensitometer in conjunction with a fringe multiplying polariscope to analyze small portions of slices from frozen stress photoelastic models [6–9]. These photoelastic results show that the stress near the loaded face tends to decrease. However, previous 3D photoelastic experimental methods have certain limitations. These experiments involved complex stress-freezing procedures such as annealing, which took a considerable amount of time. And the specific materials such as Bakelite used in photoelasticity experiments raise doubts about the applicability of the obtained results in practical applications. Besides, the axial force was added to simulate the preload force in previous studies, without considering the effect of the tightening torque on the stress distribution during the actual assembly process. Some scholars have used other means to measure bolt

☆ Project supported by National Natural Science Foundation of China (No. 12372038/12102017/92271104).
* Corresponding author.
E-mail address: bhzhaozhen@buaa.edu.cn (Z. Zhao).

https://doi.org/10.1016/j.istruc.2024.107413
Received 25 April 2024; Received in revised form 16 September 2024; Accepted 26 September 2024

stress distribution, including copper electroplating method [10], nut deformation measurement [11] and bolt deformation measurement [12]. These methods require a large number of discrete measurement points and measurement accuracy cannot be guaranteed. In recent years, ultrasonic measurement have been used for the bolt stress detection [13]. In this method, the measurement accuracy depends on the accuracy of the different algorithms. In addition, some scholars have measured the stresses for multi-bolted connections under preload [14,15]. Grzejda carried out the tests with the use of the INSTRON 8850 testing machine [16]. The courses of forces in the bolts measured with the use of resistance strain gauges and the relative displacements between the joined elements measured with an extensometer.

In addition to experimental studies, a number of scholars have investigated stress distribution in terms of theoretical modeling [17,18] and finite element (FE) simulation [19,20]. The most classic theoretical studies comes from Sopwith and Yamamoto. Sopwith developed a widely accepted load distribution model [21]. In this model, the load between the threads is considered as a concentrated force acting in the middle of the bolt thread cross-section. Sopwith compared his theoretical load distribution model with the experimental results of Goodier and Hetenyi and found them to be in general agreement. Yamamoto further expanded the analysis of the thread deformation, categorizing the elastic deformation into five types: bending deformation δ_1, shearing deformation δ_2, inclination deformation of the thread root δ_3, shearing deformation of the thread root δ_4, and deformation due to radial expansion (nut) and radial shrinkage (bolt) δ_5 [22]. Honglin Xu studied the stress distribution of casing threaded joints according to the Yamamoto method, and established a 2D FE model [23]. The theoretical results were found to be generally consistent with the FE simulation. Shikun Lu compared the stress distribution obtained from the Yamamoto model with that from a 3D FE model [24]. Comparative results indicated that both methods yield essentially the same results for load and stress distribution.

All the above studies were conducted with a given axial load on the bolt. In the actual assembly process, tightening torque needs to be applied to obtain axial preload. In order to clarify the relationship between preload force and tightening torque, contact issues during assembly need to be investigated [25]. Motosh studied the relationship between the tightening torque and axial force during bolt assmebly and found a linear proportionality between them [26], as formulated in Eq. (1).

$$T = k_{FT} F, \quad k_{FT} = \frac{p}{2\pi} + \frac{\mu_t r_t}{\cos\beta} + \mu_b r_b, \tag{1}$$

where p is thread pitch, r_t is effective thread contact radius, and r_b is effective underhead bearing radius. μ_t is coefficient of friction between threads, and μ_b is coefficient of friction between the bolt head and the contact surface. Several scholars have explored the calculation of the effective radius r_b and r_t [27–29].

With the development of optical technology, optical frequency domain reflectometry (OFDR) technique brings a new approach to stress measurement. OFDR is a kind of distributed optical fiber sensors with high spatial resolution and large dynamic range [30]. It can measure the distribution of several parameters along the tested fiber by obtaining the information about the Rayleigh scattering. As a result, OFDR can be applied to a variety of sensing scenarios, including sensing of temperature [31], strain [32], vibration [33], and 3D shape [34]. In this paper, a novel experimental approach utilizing OFDR technique is proposed to provide accurate and reliable insights into the stress or strain distribution in the bolt. Through this experiment, we expect to obtain a direct relationship between the stress distribution and the tightening torque to support the assembly process in real engineering applications. Besides, the experimental method of bolt strain measurement presented in this paper can realize the real-time measurement of bolt strain distribution, which will help monitor the internal stresses in the bolts and prevent problems such as bolt breakage under extreme loads.

Table 1
Specific parameters of the bolt.

Parameters	M20 bolt	Unit
Cross-sectional shape of bolt head	Regular hexagon	–
Side length of bolt head, a	17	mm
Thread pitch, p	2.5	mm
Thread effective diameter, d_p	18.4	mm
Thread lead angle, α	$\pi/60$	rad
Half of the thread profile angle, β	$\pi/6$	rad
Young's modulus, E	206	GPa
Poisson's ratio, ν	0.3	–
Length of engaged thread, L	48	mm

The rest of this paper is organized as follows. In Section 2, a novel experimental method using OFDR technique is proposed. The experimental equipment and preparation before the experiment are introduced. In Section 3, results of torque-preload experiment and strain distribution experiment are analyzed respectively. In Section 4, accuracy of strain distribution experiment is discussed. Comparison of experimental results with those of Yamamoto model is conducted. Finally, the conclusions are summarized.

2. Experimental preparation

The experiment setup is depicted in Fig. 1. It consists of three main modules: the bolt load operator module, the strain measurement module and the pressure sensor module. The bolt load operator module is responsible for the assembly of the bolt, including test bench, pressure sensor, bolt, PI optical fiber and other components. The test bench has a 48 mm deep threaded hole that is machined according to the ISO metric M20 thread specification. The PI optical fiber with a diameter of 0.155 mm is attached to a lathe drilled through-hole with a diameter of 5 mm inside the M20 bolt for axial deformation measurement. In order to facilitate the adhesion of the optical fiber, a guide slot with a diameter of 0.3 mm is cut in the hole through the wire-cutting process, as shown in Fig. 2. As the optical fiber is attached to the inside of the bolt, assembly torque needs to be applied to the outside of the bolt head, so the hexagon head M20 bolt is used in the experiment. Specific parameters are listed in Table 1. The pressure sensor is SA-YB-HQ/1T produced by Shiao Technology Co., Ltd. with a measuring error of less than 0.5%. The strain measurement module is used to measure the strain in the optical fiber during the assembly process. The sensing setup adopted in this module is the dynamic distributed optical fiber sensing system (OSI-D) produced by Wuhan Haoheng Technology Co., Ltd. OSI-D can achieve a spatial resolution of 1.28 mm with an measuring accuracy of about $\pm 1\,\mu\varepsilon$, which is well suited for strain measurement in a short sensing range. The sampling frequency of OSI-D can be up to 100 Hz. The pressure sensor module is used to measure the preload of the bolt. The data acquisition system used in this module is SA1808B2 produced by Shiao Technology Co., Ltd. The accuracy of the system is better than 0.5%.

Before installation, the hole and slot in the bolt, as well as the threaded portions of the bolt and the test bench, are thoroughly cleaned with an ultrasonic cleaner to remove any contaminants, such as oil from wire cutting. To ensure the accuracy of the measurement, care should be taken to ensure that the optical fiber is securely attached and free from any distortion or bending. Cyanoacrylate adhesive is used in the experiment. In the optical fiber pasting process, we place the bolt horizontally firstly, apply adhesive to the optical fiber with a guide tube along the guide slot, then spread the glue evenly with a small brush, and finally leave it for a while to allow the adhesive to fully solidify.

During installation, the test bench is fixed on the experiment table using clamps. The pressure sensor is positioned on the contact surface of the test bench to measure the preload. The bolt is tightened through the pressure sensor onto the bench using a digital torque wrench. The tightening torque can be measured by the digital torque wrench. The

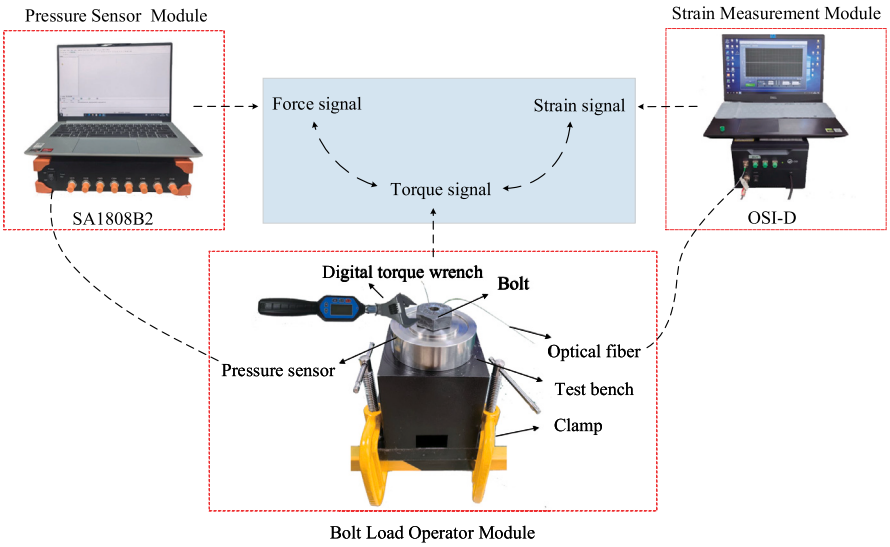

Fig. 1. Experiment setup.

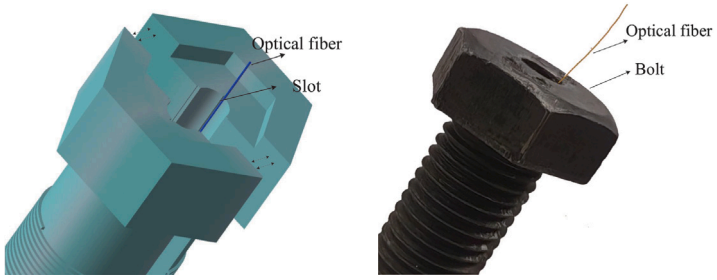

(a) Bolt profile schematic (b) Bolt sample

Fig. 2. Bolt with fiber.

pressure sensor and optical fiber are then connected to the pressure sensor module and strain measurement module, respectively. The corresponding preload and axial strain distribution can be measured at the applied torque.

After the installation of the device is completed, the experiment can be carried out. The specific experimental steps are as follows.

i. Tighten the bolt on the test bench so that the bolt is in contact with the pressure sensor, which is reading essentially 0 at this point.

ii. A torque wrench is used to increase the specified torque on the head of the bolt, and the readings of the torque wrench and pressure transducer are measured, as well as the change in strain distribution.

iii. Reverse the torque to loosen the bolt and repeat the above steps to obtain experimental data at different torques.

3. Analysis of experimental results

Since the existing classical literature basically investigates the relationship between axial tension and load distribution, in order to compare the experimental results of this paper with the existing theoretical results, the relationship between tightening torque and preload should be determined first. In this section, the experimental torque-preload curves are analyzed firstly to obtain the relationship between torque and preload. The analysis between torque and stress and strain distribution is then performed.

3.1. Torque-preload experiment

A torque-preload measurement experiment is designed to study the relationship between tightening torque and preload. This experiment is divided into two primary sections: one that incorporates the use of thrust bearings, and another that operates without them. The experimental setup without bearings is shown in the bolt load operator module in Fig. 1. Within the experimental setup involving bearings, the bearing is positioned between the pressure sensor and the bolt head. Through the use of thrust bearings, the influence of friction between the bolt head and the contact surface on the preload can be eliminated. Therefore, we can directly investigate the relationship between assembly torque and thread contact force.

In the torque-preload measurement experiment, the tightening torques from 1 N m to 9 N m are applied respectively as the experimental steps in Section 2, and the corresponding preload is measured through the pressure sensor module. Each set of experiments is repeated three times to obtain the average experimental data. The proportionality coefficient k_{FT} can thus be obtained by fitting the torque-preload curve.

The measured torque-preload curves are shown in Fig. 3. Whether or not thrust bearings are used, the preload and torque basically satisfy a linear relationship. The fitted results indicate that the maximum relative errors between the two sets of data and the corresponding

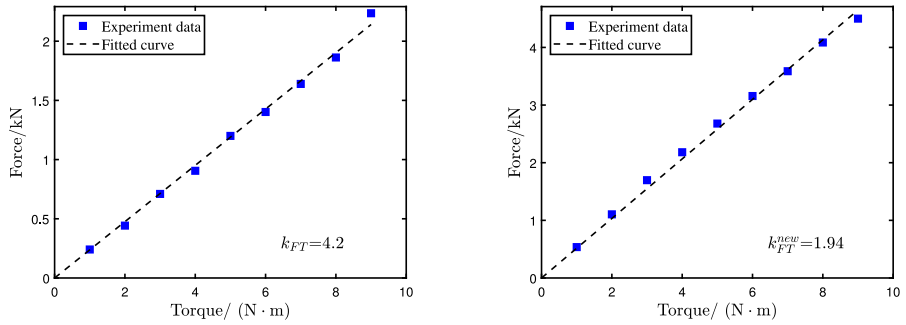

(a) Torque-preload experiment without bearings (b) Torque-preload experiment with bearings

Fig. 3. Torque-preload curves.

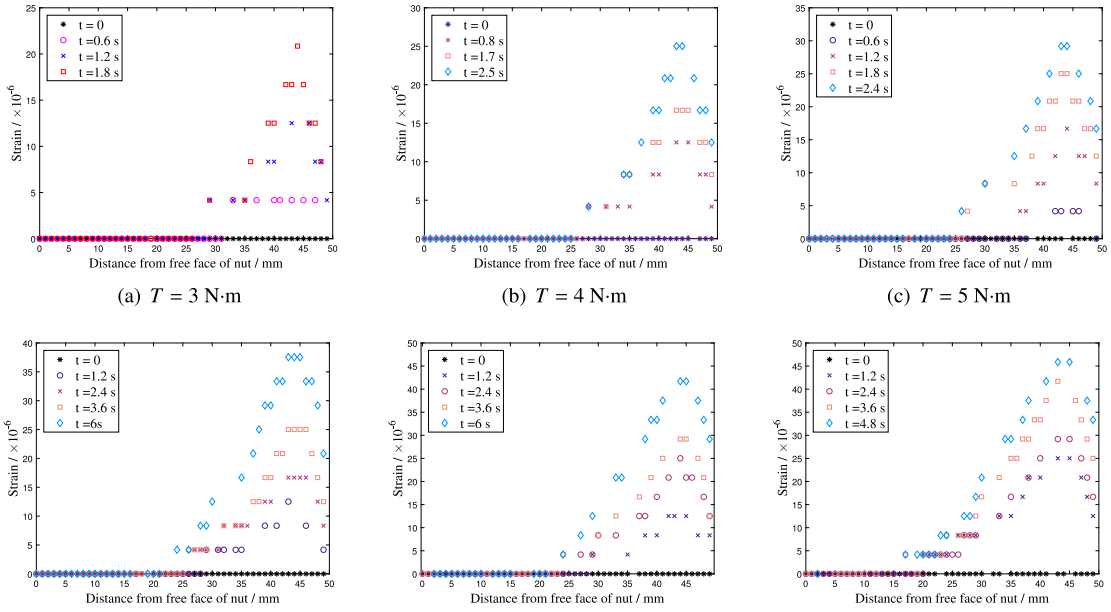

(a) T = 3 N·m (b) T = 4 N·m (c) T = 5 N·m

(d) T = 6 N·m (e) T = 7 N·m (f) T = 8 N·m

Fig. 4. The evolution of the strain distribution during assembly.

linear curves are 8.7% and 7.5%, respectively. In the torque-preload experiment without bearings, the value of proportionality coefficient k_{FT} = 4.2, while in the experiment containing bearings, the value of proportionality coefficient k_{FT} = 1.94. This result illustrates that for a given same torque, the preload obtained from the experiments with bearings is greater than the preload obtained from the experiments without bearings.

3.2. Stress distribution experiment

In this experiment, OFDR technique is used to measure the strain distribution in the axial direction of the bolt at different assembly torques ranging from 3 N m to 9 N m. After installing the experimental setup and applying the torque, the strain and stress distribution can be obtained from the strain measurement module.

The evolution of the strain distribution during assembly is shown in Fig. 4. When T = 3 N m, it can be found that the axial strain distribution law of the bolt is basically the same at different moments during the assembly process. The strain at the free boundary remains virtually negligible, whereas it gradually increases from this boundary over a range. However, a discernible reduction in strain is observed near loaded face. In addition, with the increase of torque in the assembly process, the axial strain also increases. The strain evolution law in the other torque cases is similar to that of T = 3 N m.

After obtaining the strain evolution law in the assembly history, the final strain distribution curve under different tightening torques can be extracted, and the stress distribution under different tightening torques can be obtained by Eq. (2).

$$\sigma = E\varepsilon, \tag{2}$$

$$F = A\sigma, \tag{3}$$

where A is the cross sectional area of the bolt. σ and ε are the axial stress and strain in the bolt, respectively. E denotes Young's modulus. F denotes axial force.

Comparative analysis of the stress distribution in Fig. 5(a) reveals a stress reduction phenomenon, as observed in Hetenyi's photoelastic experiments [4]. For the case of T = 3 N m, as the distance from free face increases, the stress remains around zero until the position shown by the black dashed line. Then the stress increases gradually with the distance. At a certain position near the loaded face, as shown by the red dashed line, the stress reaches a maximum value and tends to decrease gradually until the loaded face as shown by the blue dashed line. The stress distribution curves in the other cases are identical to those for T = 3 N m.

Since the thread pitch is 2.5 mm, it can be calculated that the strain decreases at one and a half thread pitch from loaded face. This may be due to the fact that the internal threads near the loaded face are not

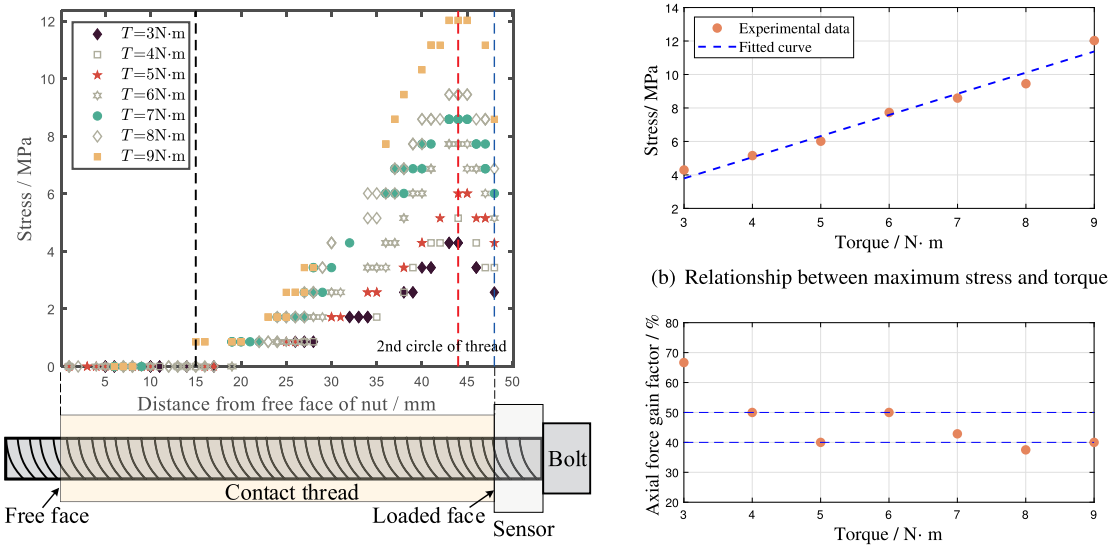

(a) Strain distribution curves for different cases

(b) Relationship between maximum stress and torque

(c) Axial force gain factor at different torques

Fig. 5. Stress distribution curves for different cases. (For interpretation of the references to color in this figure legend, the reader is referred to the web version of this article.)

Table 2
Specific parameters of the bolt.

Calculated preload/N	Experimental preload/N	Relative error/%
685.3	713.5	3.5
913.7	951.4	0.9
1142.1	1189.2	4.8
1370.5	1427.0	2.2
1598.9	1664.9	2.4
1827.3	1902.7	1.9
2284.2	2140.6	2.2

Table 3
Relevant parameters in this experiment.

Parameters	Magnitude	Unit
Cross-sectional area of nut, A_n	7834.1	mm^2
Cross-sectional area of bolt, A_b	265.9	mm^2
Sum of elastic deformation coefficients of external thread, k_b	3.576	–
Sum of elastic deformation coefficients of internal thread, k_n	4.544	–

fully formed [17], detailed analyses will be presented in Section 5. In addition, the stress in the first six threads near the free face is almost zero. This phenomenon indicates that most of the preload is carried by the first few threads of the bolt near the loaded face.

According to Eq. (3), the preload can be calculated through the stress at the loaded face. To verify the validity of the experimental stress data, the calculated preload is compared with the experimental preload in Fig. 3(a). For the case of $T = 3$ N m, the stress at the loaded face is 2.58 MPa, so that the calculated preload is 685.3 N. According to the experimental data in Fig. 3(a), the average preload is 714.3 N. Therefore, the relative error is 3.5%. The other data are presented in Table 2. The maximum relative error of these calculated preload is 4.8%, and all other relative errors are less than 3.5%, which indicates that the linear relationship obtained in Section 3.1 is well satisfied.

The maximum stress in the bolt at different torques is depicted in Fig. 5(b). After linear fitting, it can be found that the maximum stress is essentially linearly related to the torque. Since the axial force in the bolt can be calculated from the stress according to Eq. (3), it can be obtained that the maximum axial force is linearly related to the torque.

Besides, it can be observed that the maximum axial force of the bolt F_m is greater than the preload force F. After the above analysis, it can be deduced that F_m is linearly related to F. Therefore, we propose a new concept of axial force gain factor g_F, which is formulated as Eq. (4), to describe the maximum axial force in the bolt.

$$g_F = \frac{F_m - F}{F} \times 100\%. \tag{4}$$

As depicted in Fig. 5(c), axial force gain factor g_F varies essentially from 40% to 50%. That is to say, the maximum axial force in the bolt is 1.4 to 1.5 times the preload. For the case of $T = 3$ N m, $g_F = 66.7\%$. This may be due to the fact that the preload is small in this case and small errors of the same magnitude in the measurement can lead to large calculation errors.

4. Comparison with previous research

In order to verify the accuracy of the results obtained in this experiment, a comparison with the results obtained from the Yamamoto model [22] is conducted. In his research, the relationship between elongation and shortening of bolts and nuts and the deformation of the bolt threads is considered. Then the differential equation for the distribution of axial force is developed.

$$\frac{d^2F}{dx^2} = \lambda^2 F, \tag{5}$$

where λ is a constant related to material properties, as formulated in Eq. (6). The stress can then be obtained through Eq. (3).

$$\lambda = \frac{A_b + A_n}{A_b A_n (k_b + k_n) \tan\alpha}. \tag{6}$$

All relevant parameters in Eq. (5) are listed in Table 3.

The comparison with the results obtained from the Yamamoto model is conducted when the assembly torque is 3 to 6 N·m, as shown in Fig. 6. At one and a half thread pitch from the loaded face, the strain gradually decrease in the experiment, while it still increases in Yamamoto model, as depicted by the black dashed curve in Fig. 6. In addition, the experimental and theoretical curves are in good agreement until strain reduction occurs. Therefore, the Yamamoto model is in good agreement with the experimental results.

To further illustrate the accuracy of the experimental results, comparison with the photoelastic test results is conducted. It is not scientific to compare the stress curves obtained in this experiment directly with other photoelasticity tests because the material and specification of the samples used in those experiments are not exactly the same. Nevertheless, the stress concentration factor k, which is expressed as the ratio

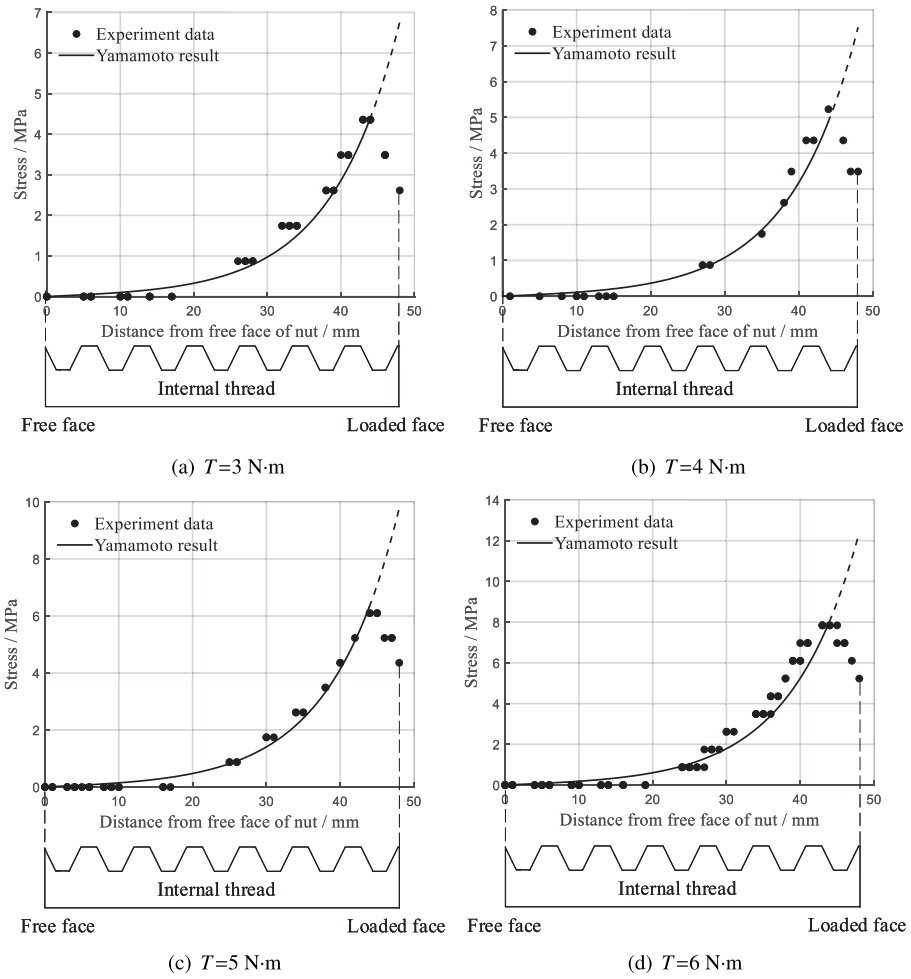

Fig. 6. Axial strain distribution.

of the axial stress to the mean axial stress in the bolt, can be used to verify experimental results. We compare the stress concentration factors derived from the experiments in this paper with those derived from Hetenyi's experiments. For T = 3 N m, the stress concentration factor rises from a value of 2.1 at the loaded face to 3.6 at one and a half thread pitch from this face. It then drops to almost zero at the free end. For T = 4 N m, the maximum stress concentration factor, k_{max} = 3.9, which is in perfect agreement with Hetenyi's result of 3.85. At other torques, k_{max} are basically between 3 and 4. These results are quantitatively consistent with Hetenyi's experiment.

Since solving the stress concentration factor requires calculating the average stress from experimental data, large errors may occur in case of insufficient data. To obtain the maximum internal force of the bolt directly from simple experiments, it is worthwhile to investigate the axial force gain factor that proposed in Section 3.2. In combination with the axial force gain factor, the maximum axial force in the bolt can be obtained by measuring the preload force through Eq. (3). The axial force gain factor in Hetenyi's experiment is calculated to be 42%, which is also in the range of 40% to 50%. This further demonstrate the accuracy of the experiment and the axial force gain factor.

5. Analysis of the causes of stress reduction

Several scholars have offered crude explanations for the phenomenon of stress reduction that occurs in experiments. This may be due to the fact that the internal threads near the loaded face of nuts are not fully formed, leading to lower thread stiffness. However, even if the thread stiffness decreases, as long as the thread contact state remains unchanged, the overall force state of the screw will not change, that is, the axial force distribution will still maintain the trend of gradually increasing. Therefore, the reason for the stress reduction needs to be further explored.

First, FE analysis is performed using the M20 thread model shown in Fig. 7. Since it is difficult to simulate bolt assembly directly using the FE method, a axial tensile model is established to simulate the bolt preload force. In the axial tension model, fixed constraint and axial tensile load are applied to the outer surface of the nut and the cross-section of the bolt, respectively, as shown in Fig. 7(a). The nut has an outer diameter of 30 mm and a length of 20 mm. The axial tension is 1000 N. Tetrahedral mesh with element size 0.5 mm is used in the thread contact area, and tetrahedral mesh with element size 1 mm is used in non-contact areas. For the stress reduction to be achieved, the part of the bolt near the loaded face must be in compression. Therefore, a local compressive force of 500 N is applied to the external thread near the contact thread of the bolt to simulate possible compression, as shown in Fig. 7(b).

The stress distribution in each number of thread on the bolt of the above two boundary conditions is shown in Fig. 8. When only axial tensile force is applied, the bolt stress increases gradually in the axial direction. When the local compressive force is added, a decrease in bolt stress occurs near the loaded face. That is, the stress reduction occurs due to local compressive force. And simple axial tension in FE model cannot generate local compression.

Based on the above analysis, the key to exploring the cause of stress reduction is to find the source of local compression. After the experiment, an upward bending deformation could be observed on the surface

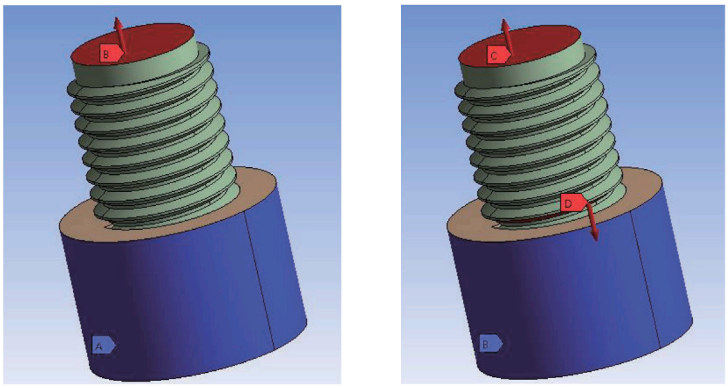

(a) Axial tension boundary (b) Local compression boundary

Fig. 7. FE simulation model.

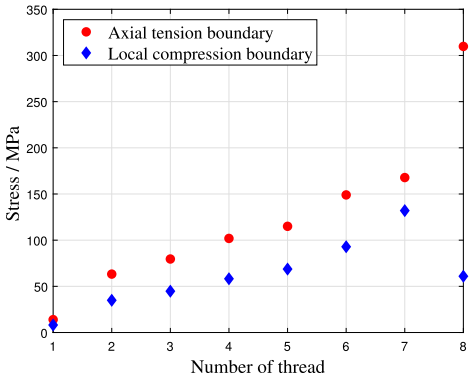

Fig. 8. Stress distribution of the bolt in FE simulation.

of the test bench, as shown in Fig. 9(a). Based on this phenomenon, we provide a preliminary explanation for the stress reduction in the bolt near the loaded face. This could be due to the fact that the internal threads are not fully formed at the boundary and therefore the stiffness is reduced, leading to increased elastic or even plastic deformation. The upper end of the internal thread then comes into contact with the lower end of the bolt thread, creating an axial force that compresses the bolt. As depicted in Fig. 9(b), the red line indicates the contact area. On the thread contact surface near the loaded face, compressive force F_c is generated, which reduces the stress in the bolt.

6. Conclusions

In this paper, a novel experimental method is proposed to investigate the stress and strain distribution in the bolt during the assembly process. With OFDR technique, the axial strain distribution of the bolt can be measured using an optical fiber affixed to the inside of the bolt.

The torque-preload curves are successfully measured through the torque-preload experiment. A linear relationship between preload force and tightening torque is obtained.

The stress distribution is revealed through the stress measurement experiment, which is consistent with the conventional photoelasticity experiment. The stress in the first six threads near the free face is almost zero. This phenomenon indicates that most of the preload is carried by the first few threads of the bolt near the loaded face. The stress start to decrease at one and a half thread pitch from loaded face. The axial force gain factor is proposed to establish the relationship between maximum axial force and preload. The maximum axial force of the bolt is basically 1.4 to 1.5 times the preload. Comparison with the Yamamoto model and Hetenyi's experiment validates the accuracy of the experiment results. In the stress rising section, the Yamamoto model is in good agreement with the experimental results. Both the stress concentration factor and the axial force gain factor in this experiment are consistent with Hetenyi's experimental results. Besides, a plausible reason for the stress reduction phenomenon is suggested and qualitatively analyzed by FE modeling.

The experimental method of bolt strain measurement presented in this paper can realize the real-time measurement of bolt strain distribution, which is of great significance for engineering application.

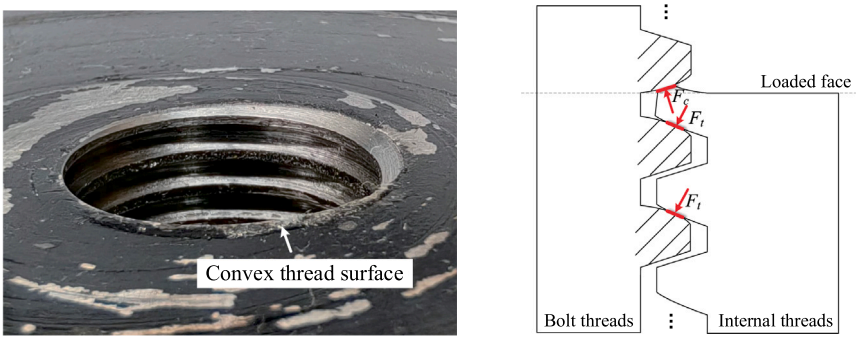

(a) Test bench surface (b) Thread contact force

Fig. 9. Thread deformation analysis.

CRediT authorship contribution statement

Zhixiang Li: Writing – review & editing, Writing – original draft, Methodology, Investigation. **Zhen Zhao:** Writing – review & editing, Supervision, Funding acquisition, Conceptualization. **Jiaying Zhang:** Supervision, Funding acquisition. **Caishan Liu:** Writing – review & editing, Supervision.

Declaration of competing interest

The authors declare that they have no known competing financial interests or personal relationships that could have appeared to influence the work reported in this paper.

References

[1] Guo H, Xie Y, Liu Y, Yang D. Study on mechanical behavior of Q690D high strength steel bearing-type bolted connections. Structures 2020;23:588–601.
[2] Ren Z, Li T, Ju Y, Cheng N, Xu J, Sheng M, Li C. Quantification of the stress field in extremely complex pores by digital photoelasticity. Measurement 2023;220:113343.
[3] Den Hartog J. The mechanics of plate rotors for turbo generators. Trans Am Soc Mech Eng 1929;51(2):1–9.
[4] Hetenyi M. A photoelastic study of bolt and nut fastenings. J Appl Mech 1943;10(2):93–100.
[5] Brown A, Hickson V. A photo-elastic study of stresses in screw threads. Proc Inst Mech Eng 1953;167(1b):605–12.
[6] Kenny B, Patterson E. Load and stress distribution in screw threads. Exp Mech 1985;25:208–13.
[7] Kenny B, Patterson E. The use of a microdensitometer in photoelastic analyses. Strain 1985;21(1):13–8.
[8] Kenny B, Patterson E. Stress analysis of some nut-bolt connections with modifications to the nut thread form. J Strain Anal Eng Des 1985;20(1):35–40.
[9] Patterson E, Kenny B. The optimisation of the design of nuts with partly tapered threads. J Strain Anal Eng Des 1986;21(2):77–84.
[10] Xu H, Shi T, Zhang Z, Shi B, et al. Loading and contact stress analysis on the thread teeth in tubing and casing premium threaded connection. Math Probl Eng 2014;2014.
[11] Goodier J. The distribution of load on the threads of screws. J Appl Mech 1940;7(1):10–6.
[12] Stoeckly E, Macke H. Effect of taper on screw-thread load distribution. Trans Am Soc Mech Eng 1952;74(1):103–12.
[13] Pan Q, Pan R, Shao C, Chang M, Xu X. Research review of principles and methods for ultrasonic measurement of axial stress in bolts. Chin J Mech Eng 2020;33(1):11.
[14] Jaszak P, Adamek K. Design and analysis of the flange-bolted joint with respect to required tightness and strength. Open Eng 2019;9(1):338–49.
[15] Grzejda R. Modern methods for modelling bolted joints at the assembly stage–A systematic review. Eng World 2023;5:97–107.
[16] Grzejda R, Kwiatkowski K, Parus A. Experimental and numerical investigations of an asymmetric multi-bolted connection preloaded and subjected to monotonic loads. Internat Appl Mech 2023;59(3):363–9.
[17] Kenny B, Patterson E. The distribution of load and stress in the threads of fasteners-a review. J Mech Behav Mater 1989;2(1–2):87–106.
[18] Shi T, Liu Y, Liu Z, Liu C. Distributions of tension and torsion in a threaded connection. Int J Mech Sci 2023;108684.
[19] TANAKA M, MIYAZAWA H, ASABA E, HONGO K. Application of the finite element method to bolt-nut joints: Fundamental studies on analysis of bolt-nut joints using the finite element method. Bull JSME 1981;24(192):1064–71.
[20] Mackerle J. Finite element analysis of fastening and joining: A bibliography (1990–2002). Int J Press Vessels Pip 2003;80(4):253–71.
[21] Sopwith D. The distribution of load in screw threads. Proc Inst Mech Eng 1948;159(1):373–83.
[22] Yamamoto A. The theory and computation of threads connection (in Japanese). Tokyo: Youkendo; 1980, p. 39–54.
[23] Brutti C. Load and stress distribution in screw threads with modified washers. J Multidiscip Eng Sci Technol 2017;4(1):6523.
[24] Lu S, Hua D, Li Y, yuan Cui F, Li P. Load and stress distribution of thread pair and analysis of influence factors. In: Journal of physics: conference series. vol. 1187, IOP Publishing; 2019, 032060.
[25] Hashimura S, Komatsu K, Inoue C, Nakao T. A new tightening method of bolt/nut assembly to control the clamping force. J Adv Mech Des Syst Manuf 2008;2(5):896–902.
[26] Motosh N. Development of design charts for bolts preloaded up to the plastic range. J Eng Ind 1976;98(3):849–51.
[27] Nassar SA, Barber G, Zuo D. Bearing friction torque in bolted joints. Tribol Trans 2005;48(1):69–75.
[28] Nassar SA, Matin PH, Barber GC. Thread friction torque in bolted joints. J Press Vessel Technol 2005;127(4):387–93.
[29] Nassar S, El-Khiamy H, Barber G, Zou Q, Sun T. An experimental study of bearing and thread friction in fasteners. J Tribol 2005;127(2):263–72.
[30] Liang C, Bai Q, Yan M, Wang Y, Zhang H, Jin B. A comprehensive study of optical frequency domain reflectometry. IEEE Access 2021;9:41647–68.
[31] Yang T, Wang X. Decoupling and simultaneous measurement of nonuniform strain and temperature using a single distributed optical fiber ring. Exp Mech 2022;62(9):1531–52.
[32] Zhang Z, Fan X, He Z. Long-range distributed static strain sensing with <100 nano-strain resolution realized using OFDR. J Lightwave Technol 2019;37(18):4590–6.
[33] Qin Z, Hu Y, Yue Y, Tan C. A dual-ended 400 km OFDR for vibration detection. Meas Sci Technol 2022;33(4):045203.
[34] Fu C, Meng Y, Chen L, Zhong H, Du C, He J, Weng X, Liu L, Qu J, Wang Y. High-spatial-resolution φ-OFDR shape sensor based on multicore optical fiber with femtosecond-laser-induced permanent scatter arrays. Opt Lett 2023;48(12):3219–22.